

Nanoscale

Accepted Manuscript

This article can be cited before page numbers have been issued, to do this please use: H. DUAN, J. Chen, F. Fianu, W. Sun and Y. Cheng, *Nanoscale*, 2026, DOI: 10.1039/D5NR05409E.



This is an Accepted Manuscript, which has been through the Royal Society of Chemistry peer review process and has been accepted for publication.

Accepted Manuscripts are published online shortly after acceptance, before technical editing, formatting and proof reading. Using this free service, authors can make their results available to the community, in citable form, before we publish the edited article. We will replace this Accepted Manuscript with the edited and formatted Advance Article as soon as it is available.

You can find more information about Accepted Manuscripts in the [Information for Authors](#).

Please note that technical editing may introduce minor changes to the text and/or graphics, which may alter content. The journal's standard [Terms & Conditions](#) and the [Ethical guidelines](#) still apply. In no event shall the Royal Society of Chemistry be held responsible for any errors or omissions in this Accepted Manuscript or any consequences arising from the use of any information it contains.

Nanoscale Protonation Limits and Charge Density in Polymer Films

Govern the Activity of Immobilized LacZ under Acid Stress

Huida Duan^{1#}, Junxing Chen^{2#}, Felicia Fianu¹,

Wei Sun^{2*}, Yifan Cheng^{1*}

1. Virginia Polytechnic Institute and State University, Department of Food Science and Technology, Blacksburg, VA 24061
2. Virginia Polytechnic Institute and State University, Department of Biochemistry, Blacksburg, VA 24061

Equal contributions

* Correspondence: Yifan Cheng (yifancheng@vt.edu), Wei Sun (sunwei@vt.edu)



1 Abstract

2 Under acidic conditions, polycationic polymer coatings can serve as protective immobilization
3 matrices that buffer local acidity and help preserve enzyme function. However, it remains
4 unclear how polymer support design parameters, particularly film thickness and effective
5 cationic charge density, govern that vital protonation process. Leveraging the nanometer-
6 scale control of film thickness and copolymer composition enabled by initiated chemical vapor
7 deposition (iCVD), we systematically investigated how these parameters govern the
8 protonation behavior of poly[glycidyl methacrylate-co-2-(dimethylamino)ethyl methacrylate]
9 (pGD) thin films and, in turn, the normalized initial ONPG hydrolysis rate of immobilized β -
10 galactosidase protein (LacZ protein). Infrared spectroscopy suggests that proton penetration
11 was capped at a depth of \sim 250 nm in pGD with 65% DMAEMA, limiting the polycationic
12 thickness in pGD films thicker than this value. Consistent with this limit, immobilized LacZ
13 activity under acidic stress (pH 4) increased with protonated thickness up to \sim 250 nm and then
14 plateaued. Raising the polycationic monomer content from 25 to 65 mol% increased LacZ
15 activity at pH 4 by up to 83%, consistent with a higher positive charge density providing
16 stronger local pH buffering. To test whether this behavior depends on immobilization methods,
17 we evaluated two approaches: random immobilization (via amine-epoxy ring-opening
18 reactions) and site-directed immobilization (via SpyCatcher/SpyTag binding). Directed
19 immobilization preserved higher LacZ activity than random immobilization, but the protonation-
20 dependent protection trend remained consistent for both strategies. Together, these results
21 identify protonation depth and charge density as orthogonal, tunable design parameters and
22 establish a thickness regime that maximizes protection without unnecessary film growth.

23
24 Key words: pH-responsive polymers, protonation, charge density, enzyme immobilization,
25 iCVD



1. Introduction

Immobilized enzymes are foundational tools in biotechnology and industrial biocatalysis, offering advantages such as enhanced stability, recoverability, and recyclability.^{1–3} Despite these advantages, maintaining the catalytic efficiency of immobilized enzymes under suboptimal environmental conditions, particularly at low pH, remains a critical challenge.^{4,5} The support material's microenvironment, especially its surface chemistry and morphology, plays a critical role in preserving enzyme activity by regulating local pH, hydrophilicity and conformational stability.^{6,7} Functional polymer coatings have emerged as versatile platforms that allow functional groups to be tailored for robust enzyme attachment, including covalent anchoring, and microenvironment modulation.^{8,9} Among these, epoxide-functionalized polymers are widely adopted for enzyme immobilization because they form stable covalent linkages with nucleophiles, such as the amines in amino acid side chains on enzyme surfaces.¹⁰

Meanwhile, pH-responsive polymers, particularly those bearing tertiary amine groups such as poly[2-(dimethylamino)ethyl methacrylate] (pDMAEMA) have shown promise in buffering local microenvironments by changing their ionization state in response to bulk pH shifts.^{11–13} For instance, pDMAEMA brushes grafted onto surfaces underwent reversible transition between collapsed (neutral) and swollen (protonated) conformations as pH changes, thereby modulating enzyme accessibility and stability.^{13,14} These materials are also advantageous due to their tunable charge density, which can be adjusted by controlling the fraction of DMAEMA in copolymer formulations.^{15–17} Together, these advancements suggest a path toward designing enzyme immobilization platforms that not only anchor enzymes but also tailor their microenvironment, particularly under pH extremes. These pH-modulating enzyme supports may benefit a variety of applications. For example, orally administered lactase must retain sufficient activity after exposure to highly acidic gastric fluids in order to remain effective during gastrointestinal transit, which has motivated the development of protected lactase delivery systems.¹⁸ Enzyme-based biosensors used for environmental and water-quality monitoring likewise operate in sample matrices where pH can vary and where pollutants such as heavy metals may compromise sensor performance.^{19,20} In addition,



1 immobilized-enzyme reactors and porous biocatalyst particles frequently develop local pH
2 gradients that differ from the bulk phase, which can reduce catalytic rates and long-term
3 stability unless the support is engineered to regulate the enzyme microenvironment.²¹ In the
4 dairy sector, lactose valorization in acid whey provides another relevant setting for robust
5 biocatalysis, because acid whey is a lactose-rich byproduct and its enzymatic upcycling into
6 lactose-hydrolyzed products, galacto-oligosaccharides, and rare sugars depends strongly on
7 maintaining sufficient β -galactosidase activity under process-relevant conditions.²² These
8 examples underscore that immobilization supports must do more than anchor enzymes
9 mechanically; they must also actively preserve a favorable local chemical environment.²³

10 Despite the promise of pH-responsive polymers for enzyme immobilization, a
11 fundamental understanding of how polymer thickness and charge density modulate
12 protonation behavior—and how this, in turn, influences biocatalytic performance—remains
13 lacking.^{24,25} In addition, while both random immobilization (e.g., amine-epoxy ring opening)
14 and (site-)directed immobilization (e.g., SpyTag/SpyCatcher binding) strategies are
15 established,²⁶ studies integrating site-specific orientation with charge-tunable polymer and
16 evaluating performance under acidic conditions remain limited. Clarifying these relationships
17 would enable more effective local pH modulation and improved activity retention of
18 immobilized enzymes under acidic conditions. Moreover, identifying the minimum
19 polycationic-support thickness required for enzyme protection would guide cost-effective
20 support design.^{19,20}

21 In this study, we derived design rules for pH-responsive polymer supports by
22 independently tuning film thickness and positive charge density. We copolymerized glycidyl
23 methacrylate (GMA, “G”) and 2-(dimethylamino)ethyl methacrylate (DMAEMA, “D”) to form
24 pGMA-co-DMAEMA (pGD) thin films, where G supplies epoxide groups for covalent protein
25 conjugation^{27,28} and D supplies tertiary amines that protonate under $\text{pH} < \text{pK}_a$ (~ 8.4) to
26 generate positive charge.⁷ To precisely control thickness and copolymer composition, we
27 synthesized these supports using initiated chemical vapor deposition (iCVD), an all-dry,
28 solvent-free vapor-deposition polymerization method^{29,30}. This method enables the formation
29 of highly conformal polymer coatings on complex and high-aspect ratio substrates due to its



1 vapor-phase, surface-limited polymerization mechanism.³¹ During the iCVD process,
2 monomer and initiator vapors (typically tert-butyl peroxide, TBPO, as the initiator) are metered
3 into a reactor held at moderate vacuum (commonly ~0.1–1 Torr).³² Monomers adsorb on a
4 cooled substrate (often ~20–40 °C), while TBPO thermally decomposes to generate radicals
5 that initiate surface-confined chain-growth polymerization.³³ As a result, iCVD enables
6 nanometer-scale thickness control and high retention of monomer functional groups (e.g.,
7 epoxides and tertiary amines) under solvent-free, mild-temperature conditions.

8 In addition to iCVD-synthesized polycationic supports, we incorporated self-assembled
9 monolayers (SAMs) bearing epoxysilane and tertiaryaminosilane to access the ultrathin limit
10 of a single molecular layer (typically ~0.5–3 nm, depending on chain length and substrate).^{34,35}
11 SAMs are a well-established, solution-phase surface modification approach for presenting
12 reactive groups and mediating covalent enzyme immobilization,^{34,36} and here they provide an
13 extreme-thickness benchmark for comparison with tens-hundreds of nm iCVD films.

14 Combining iCVD films and silane-based SAMs, we fabricated chemically parallel
15 polycationic immobilization supports with well-defined thicknesses spanning ~1 to 800 nm to
16 systematically examine protonation behavior and enzyme activity at pH 4. To probe the
17 interplay between film thickness and charge density, we varied the DMAEMA content in
18 p(GMA-co-DMAEMA) films (25% and 65%). We hypothesized that proton penetration
19 becomes self-limiting above a critical thickness because proton transport and tertiary-amine
20 protonation are coupled within a finite, structure-dependent transport zone in the film. This
21 effect, in turn, may modulate local pH buffering and the protection of immobilized enzymes
22 under acidic stress. Overall, the novelty of this work lies in decoupling two immobilization-
23 support-level design variables—effective protonated thickness and fixed positive charge
24 density—and linking them directly to the catalytic performance of immobilized LacZ under
25 acidic stress. Unlike prior studies that have typically examined pH-responsiveness or enzyme
26 orientation separately, this study probes their interplay. Leveraging the precise compositional
27 and thickness control afforded by iCVD, with SAMs as low-thickness controls, this work
28 defines a protonation limit in chemically matched polymer supports, establishes the impact of
29 this limit on enzyme protection under acid stress, and compares LacZ specific activity under



1 random and directed immobilization on the same acid-responsive platform. The specific
2 objective was therefore to derive experimentally grounded design rules for acid-protective
3 immobilization supports by relating protonation depth and charge density to LacZ activity at
4 pH 4.

5 **2. Materials and Methods**

6 **2.1 Nomenclature**

7 In this study, we employed four monomers: glycidyl methacrylate (GMA) and
8 N,N-dimethylaminoethyl methacrylate (DMAEMA) for iCVD, and 3-glycidylpropyl
9 trimethoxysilane (GPTMS) and 3-(dimethylamino)propyltrimethoxysilane (DMAPTMS) for
10 SAM coatings. We adopted a concise naming convention in which “G” denotes an
11 epoxide-bearing monomer (GMA or GPTMS) and “D” a tertiary amine monomer (DMAEMA or
12 DMAPTMS), while a leading lowercase “p” signifies an iCVD synthesized thin film and a
13 leading uppercase “S” signifies a SAM monolayer; thus, for example, pGD refers to an iCVD
14 film copolymerized from GMA and DMAEMA and SGD to a SAM composed of GPTMS and
15 DMAPTMS.

16 **2.2 Chemical reagents**

17 All reagents were used as received: the iCVD monomers glycidyl methacrylate (GMA,
18 97.0% purity with ~0.01% hydroquinone monomethyl ether stabilizer),
19 N,N-dimethylaminoethyl methacrylate (DMAEMA, 98% purity with 700–1000 ppm
20 monomethyl ether hydroquinone inhibitor) and the initiator tert-butyl peroxide (TBPO, 98%
21 purity) were obtained from Sigma-Aldrich Inc. (St. Louis, MO, USA), while the SAM reagents
22 3-glycidylpropyl trimethoxysilane (GPTMS, 98%) and 3-(dimethylamino)propyl
23 trimethoxysilane (DMAPTMS, 96%) were procured from TCI America via Fisher Scientific
24 Company LLC (Suwanee, GA, USA).

25 **2.3 Preparation of iCVD-Derived Polycationic Nanolayer Supports**

26 Polymers were deposited via iCVD to serve as LacZ immobilization supports. Glycidyl
27 methacrylate (GMA) introduced epoxy groups for covalent enzyme attachment and



1 N,N-dimethylaminoethyl methacrylate (DMAEMA) that impart pH-responsive buffering
2 capacity to the coating. Tert-butyl peroxide (TBPO) was used as the radical initiator, in line
3 with established iCVD polymerization processes.³⁷ Liquid monomers and initiator were loaded
4 in excess (>10 mL) to ensure a continuous, steady vapor supply throughout the deposition
5 duration. The deposition process was controlled by regulating vapor flow rates using needle
6 valves for the monomers and a mass flow controller (MKS Instruments, Inc.) for the initiator.
7 All precursors were vaporized and metered into the reactor at a combined flow of 3–5 sccm,
8 with TBPO held constant at 0.6 sccm. The substrate stage was maintained at 35°C under a
9 total chamber pressure of 0.6 Torr. A resistively heated filament array at 220°C generated the
10 free radicals necessary to initiate polymerization. Corning™ polystyrene 96-well plates were
11 mounted on a custom aluminum platen for efficient thermal coupling to the reactor's cooled
12 stage, and a silicon slide atop the wells allowed in situ thickness monitoring via a He–Ne
13 interferometer (350–700 nm; Thorlabs Inc., Newton, NJ, USA). Deposition parameters yielded
14 12–200 nm coatings on the Si slide ($P_{\text{m}}/P_{\text{a}} \approx 0.01$). Considering the quadratic dependence
15 of deposition rate on monomer partial pressure at low $P_{\text{m}}/P_{\text{a}}$ (<0.04 for acrylates),
16 corresponding films deposited in 96-well plates where monomer accumulation increases local
17 P_{m} , are estimated to be 50–800 nm. Detailed gas flow, $P_{\text{m}}/P_{\text{a}}$ ratios, deposition rates and
18 copolymer composition are compiled in **Tables S1, S2 and S3**.

19 **2.4 Fabrication of Self-Assembled Monolayers (SAMs)**

20 To simulate critical functional chemistries of our iCVD films, we formed mixed SAMs
21 from 3-glycidyloxypropyltrimethoxysilane (GPTMS) and
22 3-(dimethylamino)propyltrimethoxysilane (DMAPTMS) on both 96-well plates and silicon
23 wafers. Substrates were first activated by oxygen plasma (45 W, 500–900 mTorr, 3 min;
24 Harrick Plasma Inc., NY, USA) to generate surface hydroxyl groups for silane coupling.
25 Separately, 1% v/v ethanolic solutions of GPTMS and DMAPTMS were stirred at 650 rpm and
26 20°C for 1 h, then combined to yield a mixture containing 35% GPTMS and 65% DMAPTMS—
27 matching the DMAEMA fraction in the pGD(65) iCVD film. Plasma-treated substrates were
28 submerged in the GPTMS/DMAPTMS blend for 18 h at room temperature to allow silanization.



1 Finally, SAM-coated surfaces were rinsed sequentially with ethanol and deionized water and
2 dried under ambient conditions, following established processes.³⁷

3 **2.5 Ellipsometry**

4 To confirm the iCVD film thickness prior to LacZ immobilization, ex-situ measurements
5 were performed on silicon wafer samples using a J.A. Woollam alpha-SE spectroscopic
6 ellipsometer (Lincoln, NE, USA). Data were collected at three incident angles (65°, 70° and
7 75°) and fit to a Cauchy–Urbach model to extract thickness values. Each sample was
8 measured at three separate locations, and the average thickness was reported to ensure
9 consistency before proceeding with enzyme immobilization and downstream characterizations.

10 **2.6 Fourier Transform Infrared spectroscopy**

11 Fourier-transform infrared spectroscopy (FTIR) analysis was conducted to verify the
12 presence and preservation of characteristic functional groups in the polymer films synthesized
13 by iCVD. The FTIR spectroscopy of all immobilization supports was performed utilizing a
14 Thermo Scientific Nicolet iS50 Model (Austin, TX, USA). To characterize the composition of
15 copolymers, FTIR analysis was conducted in transmission mode. The experiment employed
16 attenuated total reflectance Fourier transform infrared spectroscopy (ATR-FTIR) using the
17 Thermo Scientific Nicolet iS50 Model, which was equipped with a VariGATR grazing angle
18 ATR accessory (GAT-V-N18, Harrick Scientific Products, NY). The incident angle of the ATR
19 accessory, 60°, was utilized in this study. A MCT detector cooled with liquid nitrogen was
20 utilized over the spectral range of 600–4000 cm⁻¹, with a resolution of 4 cm⁻¹. Measurements
21 were averaged over 128 scans to improve the signal-to-noise ratio. Baseline correction was
22 applied by subtracting a background spectrum obtained from an uncoated Si wafer substrate.

23 **2.7 Characterization of polymer protonation**

24 The protonation behavior of synthesized polymer films (pGD and SGD) was first
25 examined by ATR-FTIR spectroscopy. Specifically, polymer-coated substrates were
26 immersed in acidic solution (pH 4, 0.1 mM HCl) or basic solution (pH 10, 0.1 mM NaOH) for 5
27 min, followed by air-drying for 1 min. To quantify the protonation extent across polymer films



1 of varying thicknesses, FTIR spectra were additionally collected in transmission mode after
2 immersion in acidic solution (pH 4, 0.1 mM HCl) for 5 min followed by air-drying for 1 min.

3 **2.8 Bioengineering of enzymes**

4 **2.8.1 Construction of pBAD-LacZ, pBAD-LacZ-spyTag, and pBAD-SpyCatcher Expression** 5 **Plasmids**

6 The wild-type LacZ expression plasmid (pBAD-LacZ-WT) was constructed by
7 amplifying the LacZ gene (UniProt ID: P00722) via colony PCR using the primer pair LacZ-
8 WT-NdeI-F and LacZ-WT-6xHis-R. The resulting PCR product was digested with NdeI and
9 HindIII and ligated into a pBAD vector backbone pretreated with the same restriction enzymes.
10 To construct the pBAD-LacZ-spyTag plasmid, a SpyTag sequence fused to a glycine-serine
11 (GS) linker was PCR-amplified using the primers spyTag-GSlinker-F and spyTag-GSlinker-R,
12 and recombined with a LacZ-WT PCR product amplified with pBAD-LacZ-WT-spy-F and
13 pBAD-LacZ-WT-spy-R, yielding a construct with the SpyTag at the N-terminus of LacZ. For
14 the pBAD-SpyCatcher (pBAD-SC) plasmid, the SpyCatcher coding sequence (GenBank:
15 AFD50637.1) was codon-optimized and synthesized by IDT. The gene was amplified using
16 SC-NdeI-F and SC-HindIII-6xHis-R, digested with NdeI and HindIII, and ligated into a pBAD
17 vector treated with the same enzymes. Sequences of all primers used in these constructions
18 are provided in **Table S4**.

19 **2.8.2 Expression of LacZ and SpyCatcher**

20 To express wild-type LacZ (LacZ-WT), LacZ-SpyTag (LacZ-ST), and SpyCatcher (SC)
21 proteins, the plasmids pBAD-LacZ, pBAD-LacZ-SpyTag, and pBAD-SpyCatcher were
22 individually transformed into chemically competent *E. coli* DH10B cells. Transformants were
23 selected on LB agar plates containing 100 µg/mL ampicillin (LB-Amp100) and incubated
24 overnight at 37°C. A single colony from each plate was used to inoculate 5 mL of LB-Amp100
25 medium and cultured overnight at 37°C. Then, 1 mL of this preculture was transferred into 5
26 L of fresh LB-Amp100 medium. The cultures were shaken at 37°C until the optical density at
27 600 nm (OD₆₀₀) reached 0.4–0.6, and protein expression was induced by adding 0.2% (w/v)
28 L-arabinose. For LacZ-WT and LacZ-ST, induction was continued for 24 h at 37°C, while for



1 SC the culture was maintained for 24 h at 18°C to promote soluble expression. Cells were
2 harvested by centrifugation at 7000 × g for 15 min at 4°C, and the resulting cell pellets were
3 stored at –80°C until use.

4 **2.8.3 Purification of His-Tagged Proteins via Ni-NTA Chromatography**

5 Cell pellets were thawed and resuspended in 14 mL lysis buffer (20 mM Tris-HCl, pH
6 8.8, 400 mM NaCl, 20 mM imidazole, protease inhibitors), incubated at 4 °C for 30 min, and
7 lysed by sonication (Branson Sonifier 450, 50% output, pulse mode: 1 s on/off, total duration
8 15 min, with 1-min pauses every 5 min) in an ice-water bath. Lysates were clarified by
9 centrifugation (16,000 × g, 4°C, 30 min), and the supernatants incubated with 5 mL pre-
10 equilibrated HisPur™ Ni-NTA resin (Thermo Scientific) for 1 h at 4°C with continuous rotation.
11 The resin slurry was transferred onto a Poly-Prep® chromatography column, washed three
12 times with 20 mL wash buffer (20 mM Tris-HCl, pH 8.8, 400 mM NaCl, 20 mM imidazole, 2
13 mM DTT), and proteins eluted in five fractions of 3 mL each using elution buffer (20 mM Tris-
14 HCl, pH 8.8, 400 mM NaCl, 500 mM imidazole, 2 mM DTT). Eluates were concentrated via
15 Amicon Ultra-15 centrifugal filters (30 kDa cutoff for LacZ variants; 3 kDa for SC), buffer-
16 exchanged into storage buffer (20 mM Tris-HCl, pH 8.8, 400 mM NaCl, 2 mM DTT, 10%
17 glycerol) using Cytiva PD-10 Sephadex G-25M desalting columns, flash-frozen in liquid
18 nitrogen, and stored at –80°C.

19 **2.9 Enzyme immobilization**

20 For RI, LacZ-WT solution (200 µL, 0.06 mg/mL) was added to a Corning 96-well plate
21 previously coated with polymer layer. The plate was incubated statically at 37 °C for 24 h to
22 achieve covalent attachment via amine-epoxide coupling. DI proceeded in three sequential
23 steps: (i) random immobilization of SC, (ii) blocking of unreacted epoxides with glycine, and
24 (iii) site-specific capture of LacZ-ST via SC/ST interaction. Briefly, SC (200 µL, 0.05 mg/mL,
25 2.8×10^{-4} mM) was randomly immobilized under conditions identical to LacZ-WT. Remaining
26 epoxide groups were blocked using 1.0 M glycine solution following Gao et al. Subsequently,
27 LacZ-SpyTag solution (0.06 mg/mL, 1.0×10^{-4} mM) was added, and the plate was incubated
28 at 25 °C with shaking (30 rpm) for 2 h as previously described. After immobilization, residual



1 enzyme solutions were removed, wells were rinsed twice with 1× PBS to remove unbound
2 proteins, and immobilized LacZ was immediately subjected to activity assays and protein
3 quantification.

4 **2.10 Protein Quantification and Enzyme Activity Assays**

5 Protein quantification of immobilized LacZ variants was performed using a Pierce
6 bicinchoninic acid (BCA) assay kit (Thermo Fisher Scientific, Waltham, MA, USA). Briefly, 25
7 μL of 0.1 M phosphate buffer (pH 7.0) was added to each enzyme-immobilized well, followed
8 by 200 μL of BCA working reagent. Plates were mixed thoroughly for 30 s on a plate shaker
9 and incubated at 37 °C for 30 min. Protein quantification was performed for all immobilized
10 proteins, including randomly immobilized LacZ-WT, and sequentially for SC and LacZ-ST in
11 directed immobilization. Immobilization yield (IY) was calculated using the formula:

$$12 \quad IY = 100 \times C_f / C_i \%$$

13 where C_i represents the initial enzyme concentration before immobilization, and C_f is
14 the concentration equivalent of immobilized enzyme determined by the BCA assay.

15 Enzyme activity assays of immobilized and free LacZ were carried out at 37 °C using
16 o-nitrophenyl-β-D-galactopyranoside (ONPG) as substrate. Activity was measured across a
17 pH range using 0.1 M lactate buffers (pH 4) and 0.1 M phosphate buffers (pH 7). Because the
18 absorptivity of ONP/ONP⁻ at 420 nm is pH dependent, activity comparisons in this study are
19 restricted to samples measured within the same pH condition. Prior to the assays, polymer-
20 coated plates with immobilized LacZ were equilibrated at 37 °C for 10-20 min. Reactions were
21 initiated by adding ONPG solutions at concentrations of 0 and 16.6 mM. The generation of o-
22 nitrophenol was monitored at 420 nm for 5 min using a BioTek Synergy H1 Multi-Mode
23 microplate reader. The normalized initial rate v_0^* defined as the initial reaction rate measured
24 at 16.6 mM ONPG normalized by the concentration of LacZ, was employed to compare
25 enzyme activity among samples.



2.11 Enzyme Activity under Different Protonation Depths

To evaluate the influence of polymer protonation depth on the catalytic performance of immobilized enzymes, LacZ activity was measured for both RI and DI configurations on iCVD-synthesized pGD(65) films of different thicknesses (50, 100, 200, 400, 800 nm). The DI configuration served as a control to minimize orientation variability, ensuring that differences in activity reflect the microenvironmental effects induced by polymer protonation. Enzyme activity was determined at both neutral (pH 7) and acidic (pH 4) conditions. The initial reaction rate (v_0) was determined from the slope of the linear region of the absorbance–time curve and normalized to the measured protein amount. Activities were compared against free enzyme and immobilization on fully aminated SAM surfaces (SGD(65)) to distinguish protonation-driven effects from those due to surface chemistry or total charge density alone. The results were used to establish correlations between enzyme activity and the effective protonated layer thickness obtained from FTIR measurements.

2.12 Statistical analysis

All experiments were performed in triplicate ($n = 3$). Data analysis and visualization were carried out using RStudio and OriginLab, respectively. Significant differences among treatments were assessed by analysis of variance (ANOVA), followed by Tukey's Honest Significant Difference (HSD) post-hoc test to pinpoint specific differences between groups. Results were reported at a significance level of 0.05 and visualized using compact letter displays to summarize Tukey's test outcomes.

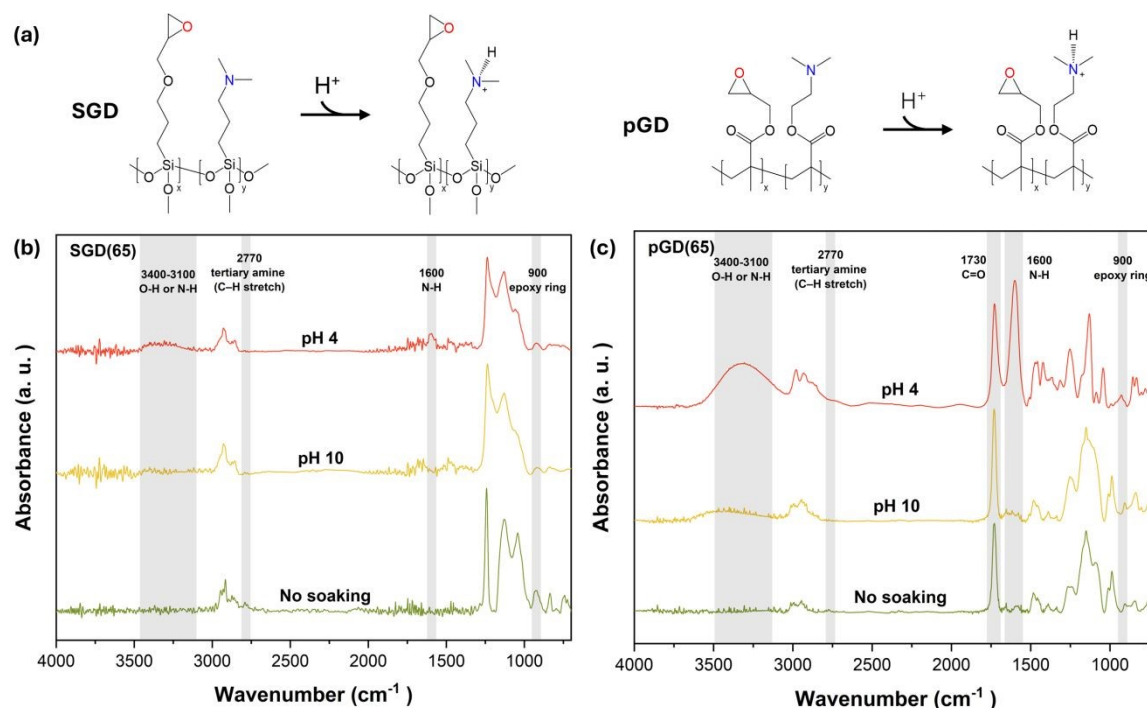
3. Results and Discussion

3.1 Characterization of immobilization supports and protonation

To illustrate the acid-induced protonation of tertiary amine groups in both pGD and SAM systems (**Figure 1a**), we first characterized the chemical structures and molar compositions of the thin films synthesized by iCVD, along with the corresponding SAMs, through FTIR spectroscopy (**Figure 1b, c**). First, we focused on several characteristic absorption peaks associated with key functional groups relevant to enzyme immobilization



1 and microenvironment modulation. The absorption peak at approximately 900 cm^{-1}
 2 corresponds to epoxide ring-deformation vibrations from the monomer glycidyl methacrylate
 3 (GMA) in pGD(65) and its SAM counterpart SGD(65).^{38–40} The presence of this peak confirms
 4 the retention of epoxide groups, which serve as critical bioconjugation sites for enzyme
 5 attachment. This mechanism is widely reported to facilitate multipoint attachment and
 6 enhanced enzyme stability and activity in immobilized systems.⁴¹



7 **Figure 1.** FTIR characterization of iCVD-synthesized thin films (pGD) and its self-assembled monolayer analog (SGD). (a) Reaction scheme showing protonation of the tertiary amine group in DMAEMA and DMAPTMS at acidic condition (pH 4). (b) FTIR spectra for SGD with 65%mol of D, SGD(65). (c) FTIR spectra for the iCVD-synthesized thin film with 65%mol of D, pGD(65).

8 Additionally, a weak absorption around 2770 cm^{-1} arises from symmetric C–H
 9 stretching vibrations of methyl groups linked to nitrogen atoms in tertiary amines. The
 10 consistent detection of this peak in both pGD(65) and SGD(65) indicates successful
 11 incorporation of tertiary amine groups derived from DMAEMA (iCVD) and DMAPTMS
 12 (SAMs).⁷ Furthermore, a strong carbonyl (C=O) stretching vibration at 1730 cm^{-1} was clearly
 13 observed in all iCVD-based polymers but absent in SAMs, confirming successful
 14 polymerization and correct structural formation. The disappearance of absorption peaks
 15 around the vinyl C=C stretch (1650 cm^{-1}) further supports complete monomer conversion



1 during iCVD synthesis. For completeness, the FTIR spectra of the individual monomers
2 (DMAEMA and GMA) together with the resulting pGD(65) film are provided in **Figure S1**,
3 where the characteristic vinyl stretching band (1650 cm^{-1}) of the monomers disappears after
4 iCVD deposition, further confirming successful polymerization.

5 To confirm protonation of the tertiary amine groups, spectra were compared before
6 and after exposure to acidic (pH 4) and basic (pH 10) solutions. Acid treatment produced two
7 new features: (i) a broad N–H stretch at $3000\text{--}3200\text{ cm}^{-1}$ and (ii) an N–H bending band near
8 $\sim 1600\text{ cm}^{-1}$, both characteristic of protonated tertiary amines. These features were absent
9 under basic conditions.⁴² Notably, these functional groups are derived from DMAEMA, whose
10 tertiary amine has a known pKa of ~ 8.4 .⁷ In polymerized form (pDMAEMA), the effective pKa
11 is somewhat lower ($7.0\text{--}7.5$) due to local electrostatic and steric effects.^{43,44} Thus, at pH 4,
12 essentially full protonation is anticipated, in alignment with the observed FTIR features.⁴⁵ In
13 contrast, the absence of these bands in basic conditions indicates deprotonation and neutrality
14 of tertiary amine groups. In addition, film thickness remained unchanged within experimental
15 error after soaking at pH 4 (**Table S5**), supporting the integrity of the pGD coatings under the
16 acid-exposure conditions used for protonation and activity assays.

17 The functional significance of these findings is substantial. Epoxide moieties ensure
18 covalent enzyme binding, while tertiary amines confer pH-responsive charge modulation.
19 Upon protonation at acidic conditions, the polymer/SAM surfaces become positively charged,
20 creating a microenvironment capable of buffering local pH and protecting immobilized
21 enzymes from external acidity. Literature documents on how buffers with ionizable groups
22 close to enzymes help preserve activity under harsh conditions by maintaining local pH and
23 shielding protein structure.⁴⁶

24 In summary, FTIR analyses (**Figure 1b, c**) clearly verify the successful incorporation
25 and preservation of epoxide functionalities essential for bioconjugation and ionizable tertiary
26 amine groups crucial for pH-responsive modulation. The acid-induced protonation verified by
27 FTIR further substantiates the pH-responsive capability of our designed polymeric supports.



1 Collectively, these structural and functional confirmations underscore the suitability of our
2 iCVD-synthesized polymer films and SAMs as advanced immobilization platforms.

3 3.2 Nanoscale Confinement of Proton Penetration

4 To further investigate how protonation varies with polycationic polymer thickness,
5 pGD(65) films with varying thicknesses were immersed in an acidic solution (pH 4, 0.1 mM
6 HCl) for 5 minutes, then air-dried for 1 minute prior to analysis. The resulting FTIR spectra
7 were analyzed (**Figure 2**). Specifically, protonation was tracked by the area ratio of the N–H
8 bending vibration peak ($\sim 1600\text{ cm}^{-1}$) relative to the carbonyl (C=O) peak ($\sim 1730\text{ cm}^{-1}$). As
9 shown in Figure 2, the protonation ratio increased with thickness up to $\sim 200\text{ nm}$, after which
10 it declined for thicker films. This observation suggests that protonation becomes transport-
11 limited in thicker films within the experimental timeframe, such that the outer film region is
12 protonated more extensively than the interior.

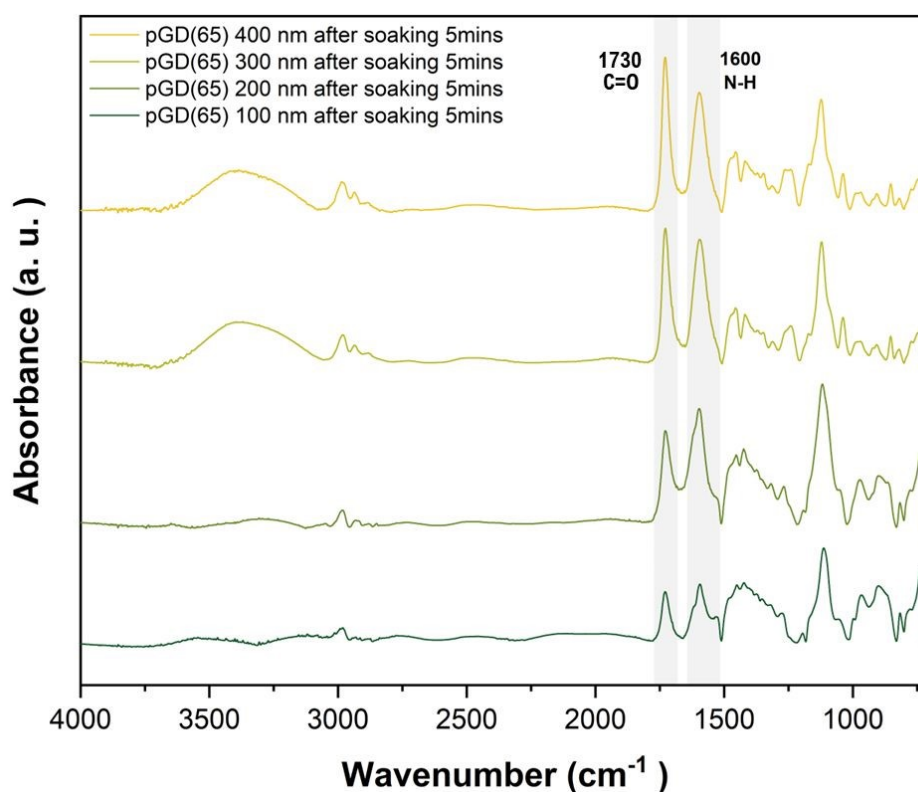


Figure 2. FTIR spectra of pGD(65) polymer films with different thicknesses after soaking in acidic solution (pH 4) for 5 min.



1 In the present pGD system, this thickness-dependent behavior seems consistent with
2 the proton-penetration-limited regime under the present experimental conditions. In hydrated
3 weak-polybase films, proton uptake is expected to arise from a coupled diffusion-reaction
4 process, in which protons migrate through water-accessible regions of the polymer while
5 tertiary amines are protonated along the transport pathway. In pGD, film thickness changed
6 little upon protonation (**Table S5**), indicating that swelling was not a major feature of the
7 present system. Accordingly, the apparent proton penetration depth in pGD is more likely
8 governed by coupled positive charge buildup and the film's transport landscape. That transport
9 landscape is defined by water-accessible free volume, local chain packing, segmental mobility,
10 and, where relevant, the degree of structural order as well as the connectivity and tortuosity
11 of transport pathways.^{47,48} These structural features can strongly influence local proton
12 diffusivity and determine whether the outer protonated region becomes kinetically resistive to
13 further inward transport. In weak polyelectrolyte layers, protonation behavior is also known to
14 depend on ionic strength, ionizable-group fraction, and polymer hydrophobicity,^{49–51} while
15 neutron-reflectivity studies further show that pH-responsive polymer brushes can exhibit
16 nonuniform internal density profiles near interfaces.⁵² We therefore interpret the ~250 nm
17 protonation plateau observed here as most likely arising from the combined effects of coupled
18 diffusion, protonation, progressive positive charge buildup, and film structure under the
19 present experimental conditions, rather than from electrostatic repulsion alone.⁵³ Because free
20 volume, porosity, and structural order were not independently measured in this study, these
21 features are treated as plausible contributors to transport limitation rather than directly
22 established properties of pGD.

23 For quantitative comparison, the N-H/C=O area ratio was calculated for each thickness
24 using FTIR spectra collected after immersion in acidic solution (pH 4, 0.1 mM HCl) for 5 min
25 followed by air-drying for 1 min. The resulting ratio for each sample was then normalized to
26 that of the fully protonated 100 nm polymer film. The integrated peak areas and normalized
27 N-H/C=O ratios used for this analysis are summarized in **Table S6**. and the corresponding
28 normalized protonation percentages for films of varying thicknesses are presented in **Figure**
29 **3**. The results indicate that polymer films thinner than 200 nm were effectively protonated



1 throughout under the present conditions, whereas thick films showed partial protonation,
 2 suggesting the maximum protonation depth lies between 200 and 300 nm. The estimated
 3 protonated layer thickness was calculated by multiplying the as-synthesized iCVD film
 4 thickness, determined by ellipsometry in ambient conditions, by the protonation degree (%)

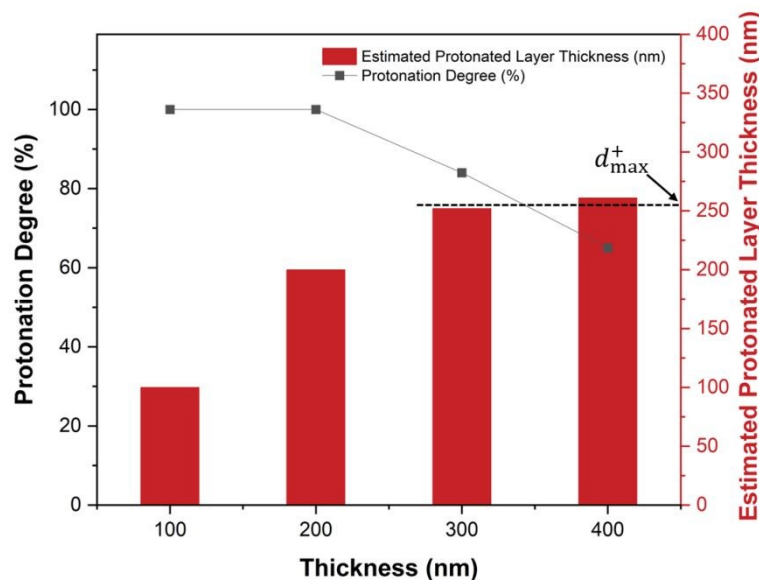


Figure 3. Normalized protonation degree (%) and estimated protonated layer thickness calculated from FTIR peak area ratios.

5 derived from FTIR spectra. The resultant estimated protonated thickness plateaued ~250 nm,
 6 which we define here as the maximum proton penetration depth (d_{max}^+) under the present
 7 exposure conditions, beyond which additional thickness no longer contributes to the
 8 protonated volume. In this estimation, swelling of the film under aqueous conditions was not
 9 explicitly taken into account.

10 3.3 Effect of Protonated Layer Thickness on Immobilized Enzyme Activity

11 Building upon the FTIR and quantitative analyses described above, which revealed a
 12 protonation depth of ~250 nm under acidic conditions, we next investigated how this
 13 protonation depth influences the catalytic performance of immobilized LacZ. **Figure 4a-d** show
 14 the catalytic activities of LacZ immobilized via random immobilization (RI) and directed
 15 immobilization (DI), along with that of soluble, surface-free LacZ as control, under both neutral
 16 (pH 7) and acidic (pH 4) conditions. These activities were normalized against the enzyme
 17 molar concentration. This approach isolates the intrinsic response of individual enzymes to



1 different microenvironments, effectively decoupling it from potential extensive effects caused
2 by difference in enzyme loading.

3 Under neutral conditions (pH 7), randomly immobilized LacZ retained only ~25% of the
4 catalytic activity of the free enzyme, suggesting that random covalent attachment to surface
5 epoxides imposed conformational constraints and steric hindrance, thereby limiting substrate
6 accessibility.⁵⁴ However, when LacZ was immobilized site-specifically through the DI, the
7 activity was significantly preserved, closely matching that of free enzyme controls. This result
8 underscores the advantage of DI over RI, highlighting that spatial orientation control
9 substantially enhances enzyme function post-immobilization by reducing structural
10 perturbation. Notably, across a support-thickness range of ~1 to 800 nm, immobilized LacZ
11 activity did not differ significantly ($p > 0.05$) for either DI or RI. Because protonation is negligible
12 at pH 7, these neutral-pH data serve as a thickness-control, indicating that properties that may
13 covary with total thickness (e.g., mechanical compliance) exert minimal influence on
14 immobilized LacZ activity.

15 Under acidic conditions (pH 4), the free LacZ showed no detectable catalytic activity,
16 consistent with prior reports that *E. coli* LacZ exhibits maximal activity near neutral pH and
17 strongly reduced activity and stability under acidic conditions.⁵⁵ Remarkably, LacZ immobilized
18 even on the SGD(65) monolayer exhibited measurable catalytic activity, indicating that a single
19 molecular layer of tertiary amines can confer electrostatic proton shielding and/or local pH
20 buffering around the enzyme. Enzyme activity increased monotonically with support thickness
21 from ~1 nm (SGD(65)) to 200 nm (pGD(65)), with a more pronounced trend for site-directed
22 immobilization (DI) than for random immobilization (RI), reflecting greater activity retention in
23 DI. Neither immobilization yield nor surface enzyme density increased monotonically with
24 support thickness (**Tables S7 and S8**), indicating that the thickness-dependent activity trend
25 under acidic conditions is not associated with enzyme loading. Beyond a polymer thickness of
26 ~200 nm (up to 800 nm), no further increase in activity was observed at pH 4 for either
27 immobilization strategy. The slightly different mean value observed for the 800 nm film does
28 not indicate a renewed thickness dependence; rather, it remains within the same plateau
29 regime as the 200 and 400 nm samples, consistent with the conclusion that only the outer



- 1 ~250 nm of the support contributes to protonation-mediated protection, while the additional
- 2 inner thickness is effectively inactive with respect to acid buffering. This plateau aligns with
- 3 the protonation-depth limit determined earlier (Section 3.2), where polymer layers thicker than
- 4 ~250 nm could not undergo additional protonation, indicating a finite proton-penetration depth.



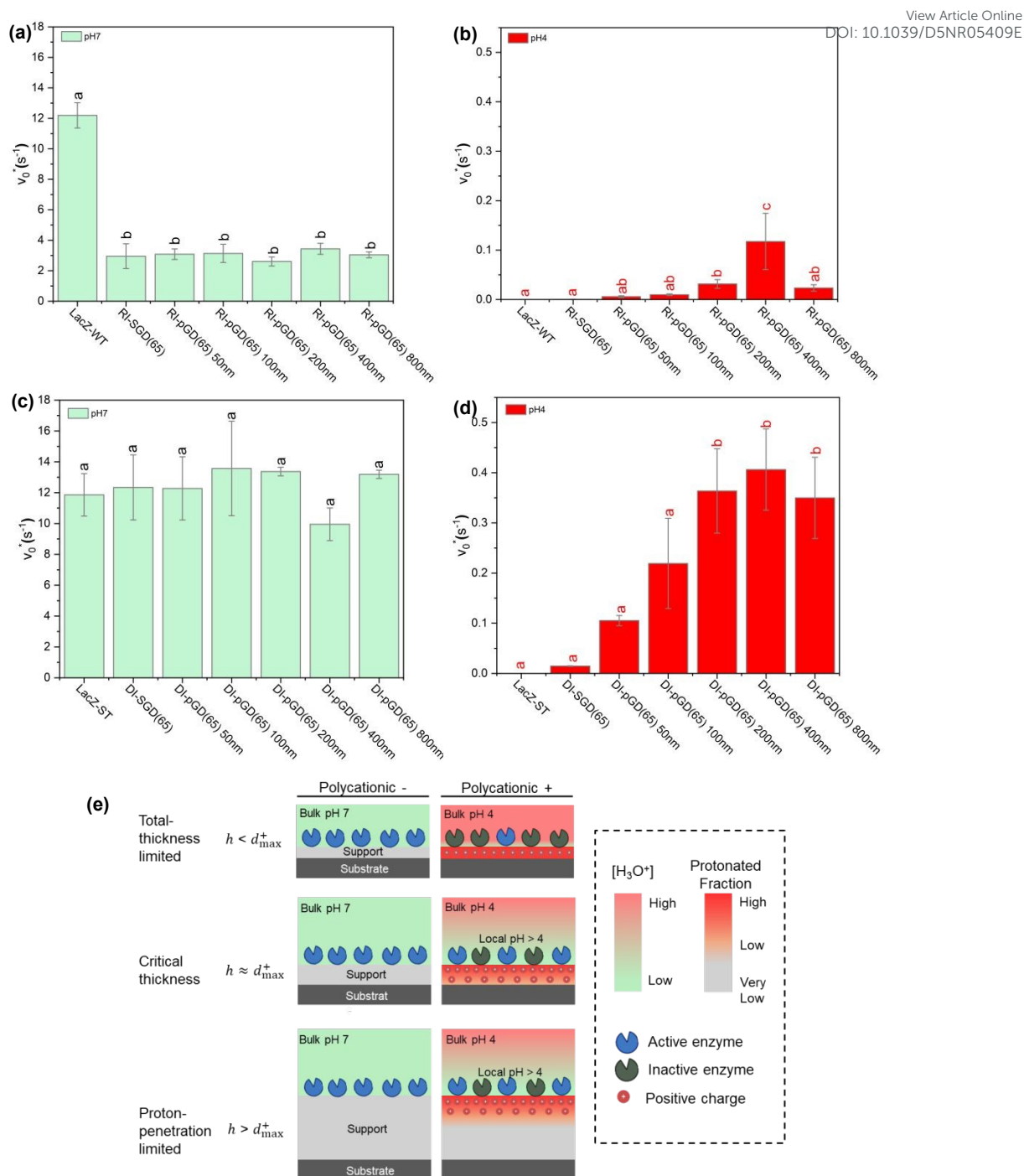


Figure 4. Effect of polymer support thickness on LacZ activity: (a,b) normalized initial rate of free and randomly immobilized LacZ-WT at pH 7 (a) and pH 4 (b); (c,d) normalized initial rate of free and directed immobilized LacZ-ST at pH 7 (c) and pH 4 (d); (e) Two-regime conceptual model defined by the relationship between total film thickness, h , and the maximum proton penetration depth, d_{max}^+ : protonation creates a positively charged microenvironment that maintains enzyme function by improving local pH compatibility at the polymer-enzyme interface.

- 1 Consequently, the activity plateau arises from the saturation of polymer protonation rather
- 2 than polymer thickness itself—once this limit is reached, additional film thickness offers



1 negligible improvement in local buffering or enzyme protection.

2 **Figure 4e** summarizes a two-regime conceptual model defined by the relationship
3 between the total thickness of the polycationic support, h , and the maximum protonation depth,
4 d_{max}^+ . When the film is thinner than the protonation depth ($h < d_{max}^+$), protons can fully
5 penetrate the support and convert tertiary amines into protonated tertiary ammonium groups,
6 placing the system in a **total-thickness-limited regime** (top row). In this regime, very thin
7 supports (e.g., SGD) provide weak proton shielding, whereas increasing h increases the
8 amount of protonated polycationic material and correspondingly enhances LacZ activity under
9 acidic stress.

10 As the film thickness approaches the protonation limit ($h \approx d_{max}^+$; middle row), the
11 entire support becomes protonated. Further increases in h no longer increase the protonated
12 thickness, defining an optimal or “sweet-spot” thickness that maximizes enzyme protection
13 while minimizing coating material usage and deposition time.

14 When the support thickness exceeds the protonation depth ($h > d_{max}^+$; bottom row),
15 the system enters a **proton-penetration-limited regime**, in which the protonated layer
16 thickness remains constant despite additional film growth. Consequently, further increases in
17 total thickness do not improve the acid resistance of immobilized LacZ.

18 Collectively, these results explicitly demonstrate that the protonation depth, rather than
19 the absolute polymer thickness, determines the extent to which local buffering can protect and
20 preserve enzyme activity under acidic conditions. Controlling polymer thickness within the
21 protonation saturation limit (around 200–300 nm) emerges as a critical strategy for optimizing
22 enzyme immobilization systems for acidic biocatalytic applications.

23 **3.4 Influence of Polycationic Monomer density on Immobilized Enzyme Activity**

24 Beyond polymer thickness, the molar ratio of protonatable monomers within polymer
25 formulations could influence the catalytic activity of immobilized enzymes. To systematically
26 investigate this effect, we synthesized copolymers with different compositions of DMAEMA
27 monomer, specifically pGD(25) and pGD(65), representing lower and higher polycationic



1 monomer ratio. Enzyme activities were measured across polymer films of varying thicknesses
 2 (200 nm, 400 nm, 800 nm), and results are summarized in **Figure 5**.

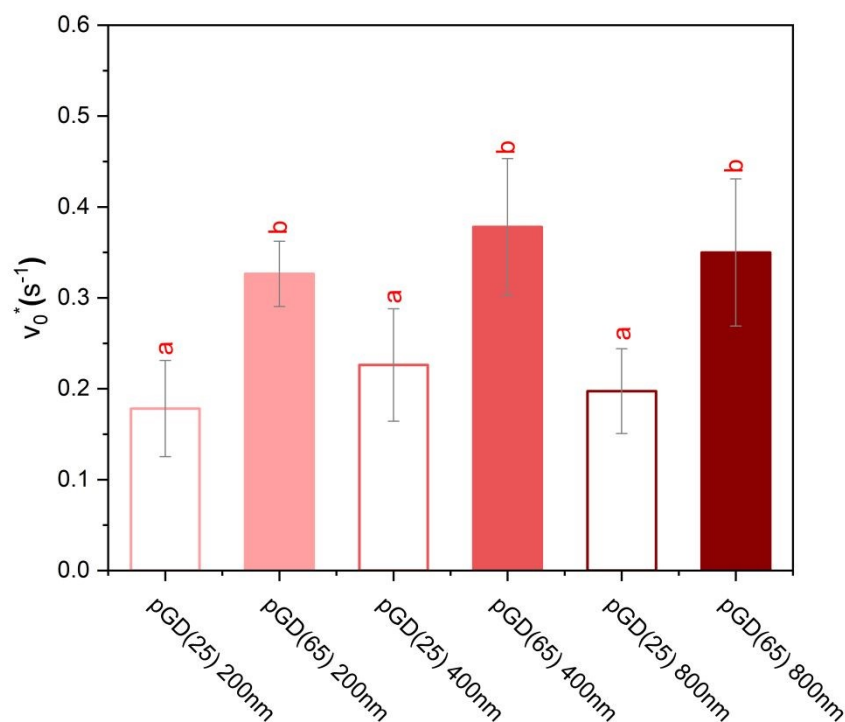


Figure 5. Normalized activities of immobilized LacZ on polymer films with varying thicknesses and compositions, evaluated at pH 4.

3 **Figure 5** shows that for a given polymer composition (either pGD(25) or pGD(65)), no
 4 statistically significant difference in enzyme activity was observed among films of different
 5 thicknesses. This outcome is consistent with previous observations that, beyond a certain
 6 thickness (where protonation saturation occurs), further increases in polymer thickness alone
 7 do not influence enzyme activity. However, when we compare enzyme activities immobilized
 8 on polymers with different polycationic compositions, a pronounced difference emerged.
 9 Specifically, enzyme activity on pGD(65) was significantly higher, 83% greater—than on
 10 pGD(25) at all tested thicknesses. This notable increase can be attributed to the substantially
 11 higher density of protonatable tertiary amine groups present in pGD(65), providing a stronger
 12 local buffering capacity. The underlying mechanism for this protective effect is based on the
 13 protonation of tertiary amines under acidic conditions, as indicated by our earlier FTIR results
 14 (Section 3.1). Protonation results in a positively charged polymer region that alters local ion
 15 partitioning and reduces proton access to the immobilized enzyme, thereby enhancing local



1 buffering under acidic conditions. Nearly all tertiary amines (~99.99%) in DMAEMA-based
2 polycationic polymer (pKa ~8.4) are protonatable at pH 4, notwithstanding the aforementioned
3 self-limiting protonation depth behavior. Therefore, the increased DMAEMA content in pGD(65)
4 generates a higher local positive charge density, offering more effective electrostatic repulsion
5 and stronger local buffering capability. Consequently, enzyme immobilized on pGD(65)
6 experienced substantially less acidic stress compared to those on lower-DMAEMA-content
7 polymers such as pGD(25). Our findings align well with previous studies reporting similar
8 protective effects conferred by positively charged polymer supports (e.g., polyethylenimine
9 and chitosan), which have demonstrated significant enzyme activity retention or even
10 enhancements upon immobilization under non-optimal pH conditions.^{56,57}

11 From a catalytic perspective, this protection likely arises because the polycationic
12 support helps preserve a more favorable local ionization environment around the LacZ active
13 site under acidic bulk conditions. *E. coli* LacZ protein follows a double-displacement
14 mechanism involving two essential glutamate residues, Glu461 and Glu537, which function
15 as the general acid/base catalyst and nucleophile, respectively.^{58–61} A schematic summary of
16 the LacZ catalytic residues and their expected acid sensitivity is provided in **Figure S2**. Under
17 strongly acidic conditions, excessive proton activity is expected to suppress the catalytic roles
18 of these carboxylate residues, thereby impairing ONPG hydrolysis.^{58–61} In addition to this
19 active-site effect, our Circular Dichroism (CD) measurements showed a marked loss of
20 ellipticity at 208 and 222 nm at pH 4, consistent with reduced α -helical content and partial
21 structural destabilization (**Supporting Methods**). The corresponding CD spectra are shown
22 in **Figure S3**. These observations suggest that acid-induced deactivation of LacZ arises from
23 both catalytic-residue protonation and global conformational disruption. In this context, the
24 protonated DMAEMA-containing support does not directly activate the enzyme; rather, it likely
25 attenuates proton influx and buffers the local environment surrounding the immobilized
26 enzyme, helping maintain both catalytic competence and structural integrity.²¹ Increasing
27 protonated thickness and/or positive charge density expand this protective region until the
28 proton penetration limit is reached, whereas increasing DMAEMA content increases the
29 density of protonatable groups within that region and thereby strengthens the buffering effect.



1 The practical implication of this result is that, once the film is sufficiently thick to
2 establish a protonated interfacial buffering layer, increasing charge density becomes a more
3 effective design parameter than further increasing total thickness. In this context, the 83%
4 enhancement in LacZ activity observed for pGD(65) relative to pGD(25) is not merely
5 incremental, but functionally significant, as it reflects a substantial recovery of catalytic
6 performance under acidic conditions (pH 4), where free or weakly protected enzymes typically
7 exhibit severely diminished activity. Importantly, this improvement is achieved without
8 increasing film thickness, which would otherwise introduce additional mass-transfer resistance
9 and prolong deposition time. Because only two DMAEMA levels were tested, the present data
10 establish the trend but do not define its upper limit. Increasing %D further may improve acid
11 protection, but likely with a tradeoff in enzyme loading as %G decreases. Future work may
12 therefore optimize composition from the perspective of total catalytic activity. Taken together,
13 these results show that enriching protonatable amine content provides an complementary
14 acid-protection route to increasing thickness, providing another degree of freedom to balance
15 catalytic performance with practical constraints such as fabrication throughput, material usage,
16 and substrate diffusion.

17 More broadly, these findings suggest a generalizable support-design principle for acid-
18 stressed biocatalysis: a minimum thickness is first required to establish a protonated interfacial
19 region, beyond which further performance gains are more effectively achieved by tuning local
20 charge density rather than adding inactive material. This strategy is directly relevant to
21 systems where enzymes must retain activity in acidic or pH-variable environments, including
22 oral lactase delivery through gastric conditions, biosensing platforms operating in complex or
23 unbuffered samples, immobilized-enzyme reactors where local pH gradients can arise during
24 catalysis, and LacZ-driven lactose valorization in acid whey and related biomanufacturing
25 processes, where a mismatch often exists between the bulk feed conditions and the optimal
26 pH window of the enzyme.



1 Conclusion

2 This study provides a framework for understanding the effect of protonation depth and
3 charge density on polycationic polymer support, and in turn, on enzyme activity under acidic
4 conditions. By combining iCVD and SAM immobilization supports with precisely controlled
5 thickness and tunable copolymer composition, we systematically investigated how film
6 thickness and the molar ratio of protonatable monomers (DMAEMA) influence the spatial
7 distribution and extent of protonation.

8 We demonstrated that at pH 4 protonation in pGMA-co-DMAEMA (DMAEMA~65%mol)
9 films is confined to a finite nanoscale depth of ~250 nm, which we term d_{max}^+ , a material
10 parameter that dictates the upper limit of enzymatic protection under the tested conditions. A
11 two-regime model can be defined based on d_{max}^+ : when protonatable film thickness is smaller
12 than d_{max}^+ , the system is in a total-thickness-limited regime; when protonatable film thickness
13 is greater than d_{max}^+ , the system is placed in a proton-penetration-limited regime. By
14 correlating this depth with the activity of immobilized LacZ, we showed that matching film
15 thickness to this saturation limit is essential for efficient design: d_{max}^+ defines an optimal or
16 “sweet-spot” thickness that maximizes enzyme protection while minimizing coating material
17 usage and deposition time. Furthermore, while site-directed immobilization offers better
18 absolute performance by preserving enzyme orientation, the protective buffering mechanism
19 is eventually governed by the polymer's charge density and protonation depth. These findings
20 shed light on protonation depth and charge density as physicochemical design parameters for
21 developing functional polycationic immobilization supports for enzyme-based biocatalysis,
22 biosensors, and biomedical systems.

23 Acknowledgement

24 Y.C. acknowledges the support of the Foundation for Food and Agriculture Research
25 (FFAR) New Innovator Award (23-000576) and award No. USDA NIFA 2021-67034-35040
26 and start-up funds provided by Virginia Tech for this work. W.S. acknowledges support from
27 start-up funds provided by Virginia Tech. J.C. acknowledges support from the Virginia Tech



- 1 Biochemistry Graduate Program. The authors thank members of the Cheng and Sun
2 laboratories for technical assistance and constructive feedback.
3

View Article Online
DOI: 10.1039/C5NR05409E



Reference

- 1 1 S. M. Mirsalami, M. Mirsalami and A. Ghodousian, *Results Chem.*, 2024, **7**, 101486.
- 2 2 F. Asaduzzaman and S. Salmon, *Mol. Syst. Des. Eng.*, 2022, **7**, 1385–1414.
- 3 3 J. M. Guisan, G. Fernandez-Lorente, J. Rocha-Martin and D. Moreno-Gamero, *Curr. Opin. Green Sustainable Chem.*, 2022, **35**, 100593.
- 5 4 Y. R. Maghraby, R. M. El-Shabasy, A. H. Ibrahim and H. M. E. S. Azzazy, *ACS Omega*, 2023, **8**, 5184–5196.
- 7 5 M. S. Robescu and T. Bavaro, *Molecules*, 2025, **30**(4), 939.
- 8 6 M. G. Holyavka and V. G. Artyukhov, *Biophys. Rev.*, 2025, 1–39.
- 9 7 P. Cotanda, D. B. Wright, M. Tyler and R. K. O'Reilly, *J. Polym. Sci. A Polym. Chem.*, 2013, **51**, 3333–3338.
- 11 8 W. A. A. Wahab, *Microb. Cell Fact.*, 2025, **24**, 167.
- 12 9 X. Lyu, R. Gonzalez, A. Horton and T. Li, *Catalysts*, 2021, **11**, 1211.
- 13 10 T. Prabhakar, J. Giaretta, R. Zulli, R. J. Rath, S. Farajikhah, S. Talebian and F. Dehghani, *Chem. Eng. J.*, 2025, **503**, 158054.
- 15 11 G. Kocak, C. Tuncer and V. Bütün, *Polym. Chem.*, 2017, **8**, 144–176.
- 16 12 J. Zdarta, A. S. Meyer, T. Jesionowski and M. Pinelo, *Catalysts*, 2018, **8**(2), 92.
- 17 13 H. Zhou, X. Wang, J. Tang and Y. W. Yang, *Polymers*, 2016, **8**, 277.
- 18 14 S. N. H. Ishak, A. H. M. Saad, W. Latip, R. N. Z. R. A. Rahman, A. B. Salleh, N. H. A. Kamarudin, A. T. C. Leow and M. S. M. Ali, *Int. J. Biol. Macromol.*, 2025, **316**, 144278.
- 20 15 A. Vardaxi and S. Pispas, *Polymers*, 2023, **15**, 1519.
- 21 16 X. Fu, L. Hosta-Rigau, R. Chandrawati and J. Cui, *Chem*, 2018, **4**, 2084–2107.
- 22 17 J. Niskanen, C. Wu, M. Ostrowski, G. G. Fuller, S. Hietala and H. Tenhu, *Macromolecules*, 2013, **46**, 2331–2340.
- 24 18 K. C. Kwon, D. Verma, N. D. Singh, R. Herzog and H. Daniell, *Adv. Drug Deliv. Rev.*, 2013, **65**, 782–799.
- 26 19 A. P. F. Turner, *Chem. Soc. Rev.*, 2013, **42**, 3184.
- 27 20 B. L. Vallee and D. D. Ulmer, *Annu. Rev. Biochem.*, 1972, **41**, 91–128.
- 28 21 R. A. Sheldon and S. van Pelt, *Chem. Soc. Rev.*, 2013, **42**, 6223–6235.
- 29 22 P. Kolev, D. Rocha-Mendoza, S. Ruiz-Ramírez, J. Ortega-Anaya, R. Jiménez-Flores and I. García-Cano, *JDS Communications*, 2022, **3**, 1–6.
- 31 23 C. Mateo, J. M. Palomo, G. Fernandez-Lorente, J. M. Guisan and R. Fernandez-Lafuente, *Enzyme Microb. Technol.*, 2007, **40**, 1451–1463.
- 33 24 S. Tippner, D. Hernández-Castillo, F. H. Schacher and L. González, *J. Phys. Chem. B*, 2025, **129**, 2105–2114.
- 35 25 X. Laloyaux, B. Mathy, B. Nysten and A. M. Jonas, *Macromol.*, 2010, **43**, 7744–7751.
- 36 26 X. Pei, Z. Luo, L. Qiao, Q. Xiao, P. Zhang, A. Wang and R. A. Sheldon, *Chem. Soc. Rev.*, 2022, **51**, 7281–7304.
- 38 27 M. Gupta and K. K. Gleason, *Thin Solid Films*, 2006, **515**, 1579–1584.
- 39 28 Y. H. Youn, S. J. Lee, G. R. Choi, H. R. Lee, D. Lee, D. N. Heo, B. S. Kim, J. B. Bang, Y. S. Hwang, V. M. Correlo, R. L. Reis, S. G. Im and I. K. Kwon, *Mater. Sci. Eng. C*, 2019, **100**, 949–958.
- 41 29 K. K. Gleason, *Nat. Rev. Phys.*, 2020, **2**, 347–364.



- 1 30 K. K. Gleason, *Adv. Mater.*, 2024, **36**(8): 2306665. View Article Online
DOI: 10.1039/D5NR05409E
- 2 31 K. Park, K. K. Gleason and R. Yang, *Adv. Funct. Mater.*, DOI:10.1002/adfm.202417620.
- 3 32 Y. Cheng, A. Khlyustova, P. Chen and R. Yang, *Macromol.*, 2020, **53**, 10699–10710.
- 4 33 K. K. S. Lau and K. K. Gleason, *Macromol.*, 2006, **39**, 3688–3694.
- 5 34 I. Luzinov, D. Julthongpiput, A. Liebmann-Vinson, T. Cregger, M. D. Foster and V. V
6 Tsukruk, *Langmuir*, 2000, **16**, 504–516.
- 7 35 J. C. Love, L. A. Estroff, J. K. Kriebel, R. G. Nuzzo and G. M. Whitesides, *Chem. Rev.*,
8 2005, **105**, 1103–1170.
- 9 36 S. Libertino, F. Giannazzo, V. Aiello, A. Scandurra, F. Sinatra, M. Renis and M. Fichera,
10 *Langmuir*, 2008, **24**, 1965–1972.
- 11 37 Jean. Pinson and Damien. Thiry, *Surface modification of polymers: methods and
12 applications*, Wiley-VCH, 2019.
- 13 38 I. D. Vukoje, E. S. Džunuzović, V. V. Vodnik, S. Dimitrijević, S. P. Ahrenkiel and J. M.
14 Nedeljković, *J. Mater. Sci.*, 2014, **49**, 6838–6844.
- 15 39 M. Sobiesiak, *Adsorption*, 2019, **25**, 257–266.
- 16 40 H. Shivhare, *SSRN Electron. J.*, 2024, DOI: 10.2139/ssrn.5163538.
- 17 41 C. Mateo, V. Grazú, G. Grazú, B. C. C. Pessela, T. Montes, J. M. Palomo, R. Torres, F. L.
18 Opez-Gallego, R. Fernández, F. Fernández-Lafuente, J. M. Guisán and G. Guisán,
19 *Biochem. Soc. Trans.*, 2007, **35**, 1593–1601.
- 20 42 B. Smith, *Spectroscopy*, 2019, **34**, 30–37.
- 21 43 E. W. Kent, E. M. Lewoczko and B. Zhao, *Polym. Chem.*, 2021, **12**, 265–276.
- 22 44 J. C. Y. Wu, C. H. Hutchings, M. J. Lindsay, C. J. Werner and B. C. Bundy, *J. Biotechnol.*,
23 2015, **193**, 83–90.
- 24 45 R. A. Heacock and L. Marion, *Can. J. Chem.*, 1956, **34**, 782–1795.
- 25 46 F. Stoffel, M. Papp, M. Gil-Garcia, A. M. Küffner, A. I. Benítez-Mateos, R. P. B. Jacquat, N.
26 Galvanetto, L. Faltova and P. Arosio, *Nat. Commun.*, 2025, **16**, 6368.
- 27 47 J. Sharma, K. Tewari and R. K. Arya, *Prog. Org. Coat.*, 2017, **111**, 83–92.
- 28 48 A. Mansuri, M. Völkel, T. Feuerbach, J. Winck, A. W. P. Vermeer, W. Hoheisel and M.
29 Thommes, *Macromol.*, 2023, **56**, 3224–3237.
- 30 49 J. D. Willott, T. J. Murdoch, B. A. Humphreys, S. Edmondson, G. B. Webber and E. J.
31 Wanless, *Langmuir*, 2014, **30**, 1827–1836.
- 32 50 S. Ramezani Bajgiran, F. Safi Samghabadi, S. Li, J. C. Conrad and A. B. Marciel, *Macromol.*,
33 2023, **56**, 9218–9228.
- 34 51 J. D. Willott, B. A. Humphreys, T. J. Murdoch, S. Edmondson, G. B. Webber and E. J.
35 Wanless, *Phys. Chem. Chem. Phys.*, 2015, **17**, 3880–3890.
- 36 52 M. Moglianetti, J. R. P. Webster, S. Edmondson, S. P. Armes and S. Titmuss, *Langmuir*,
37 2010, **26**, 12684–12689.
- 38 53 G. Ferrand-Drake del Castillo, R. L. N. Hailes and A. Dahlin, *J. Phys. Chem. Lett.*, 2020,
39 **11**, 5212–5218.
- 40 54 M. J. Paiva, F. C. Paula-Elias, L. A. Pereira, S. C. Carreiro, E. C. Vieira-Almeida, E. M.
41 Silva, G. S. Dias, M. A. C. Xavier, S. A. Morales, R. F. Perna and A. F. Almeida, *J. Braz.
42 Chem. Soc.*, 2023, **34**, 1743–1752.
- 43 55 A. A. Hamed, M. Khedr and M. Abdelraof, *J. Genet. Eng. Biotechnol.*, 2020, **18**, 80.
- 44 56 J. J. Virgen-Ortíz, J. C. S. Dos Santos, Á. Berenguer-Murcia, O. Barbosa, R. C. Rodrigues



- 1 and R. Fernandez-Lafuente, *J. Mater. Chem. B*, 2017, **5**, 7461–7490.
- 2 57 W. Wang, N. Guo, W. Huang, Z. Zhang and X. Mao, *Catalysts*, 2018, **8**, 401.
- 3 58 J. Yuan, M. Martinez-Bilbao and R. E. Huber, *Biochem. J.*, 1994, **299**, 527–531.
- 4 59 J. C. Gebler, R. Aebersold and S. G. Withers, *J. Biol. Chem.*, 1992, **267**, 11126–11130.
- 5 60 J. P. Richard, R. E. Huber, S. Lin, C. Heo and T. L. Amyes, *Biochemistry*, 1996, **35**, 12377–
6 12386.
- 7 61 C. G. Cupples, J. H. Miller and R. E. Huber, *J. Biol. Chem.*, 1990, **265**, 5512–5518.
- 8



Data Availability Statement

All data supporting the results of this study (including experimental measurements, spectra, polymer characterization data, and any other datasets analyzed during this work) are provided in the Supporting Information accompanying this article.

